Available online at www.sciencedirect.com
ScienceDirect
Journal of Power Sources 165 (2007) 844–853
JOURNAL OF POWER SOURCES
www.elsevier.com/locate/jpowsour

1 kW_e sodium borohydride hydrogen generation system Part I: Experimental study

Jinsong Zhang, Yuan Zheng *, Jay P. Gore, T.S. Fisher

School of Mechanical Engineering, The Energy Center at Discovery Park, Purdue University, West Lafayette, IN 47907-2014, USA

Received 13 November 2006; received in revised form 20 December 2006; accepted 20 December 2006
Available online 9 January 2007

Abstract

A 1 kW_e hydrogen generation system using hydrolysis of sodium borohydride ($NaBH_4$) has been designed and built. The effects of flow rate, fuel concentration, inlet temperature and operating pressure on chemical conversion have been systematically investigated. A 10-point thermocouple profile probe was used to measure the temperature distribution inside the catalyst bed. Chemical conversion was also qualitatively evaluated via the temperature profile. For the present adiabatic reactor, a large temperature gradient at the outlet implies low conversion, while a small temperature gradient at the outlet implies high conversion. In order to obtain accurate measurements of hydrogen flow rate, water vapor carried in the product stream was removed by a custom hydrogen conditioning station. Using 15% concentration $NaBH_4$ aqueous solution, this system generated hydrogen up to 20 SLPM with a reasonably high chemical conversion (95%). Discharge products from using $NaBH_4$ concentrations above 15% crystallized upon cooling to room temperature. Such products would be difficult to remove from the discharge tank in a practical setting. Considering the practical difficulties in heating the discharge product to prevent crystallization, the highest usable concentrations would likely fall in the range of 10–15%. The resulting maximum material gravimetric density is 3.1 wt% of hydrogen and falls short of the DOE on-board hydrogen storage system target of 6 wt% for year 2010.

Keywords: Hydrogen storage; Sodium borohydride; Crystallization; Liquid catalysis

1. Introduction

Hydrogen has been identified as a promising energy carrier for the future because it offers the potential for fuel-efficient, emissions-free vehicles and can be produced from multiple primary energy sources. Utilizing hydrogen produced from renewable sources in fuel cells or internal combustion engines offers the potential to reduce greenhouse gas emissions and pollution. Nevertheless, many critical technical challenges need to be overcome before a hydrogen-based energy economy could become viable [1,2]. On-board hydrogen storage is one of the most challenging technical barriers to the implementation of the hydrogen economy. To achieve reasonable fuel efficiency and allow adequate cargo space, weight and volume for on-board hydrogen storage system must be limited. As a result, the U.S. Department of Energy's Freedom Car Program targets [2] dictate that the gravimetric density of a hydrogen storage system should be at least 6 wt.% (i.e., 6 kg H_2 in a 100 kg tank), and the volumetric density should be at least 45 g H_2 L^{-1} by 2010. The targets for 2015 are 9 wt.% for gravimetric density and 81 g H_2 L^{-1} for volumetric density.

Existing hydrogen storage methods include compressed hydrogen, liquid hydrogen, metal hydrides and chemical hydrides [3]. Sodium borohydride systems have attracted much attention because of their intrinsic safety and easy handling of fuel compared to other options. This concept was first proposed by Millennium Cell Inc. [4,5]. Most chemical hydrides react with water violently upon contact, but sodium borohydride is an exception. Sodium borohydride reacts rapidly with water (hydrolysis) only in the presence of catalyst, normally ruthenium metal or ruthenium salt, as

$$NaBH_4 + 2H_2O \xrightarrow{\text{catalyst}} NaBO_2 + 4H_2 + \text{heat} \quad (1)$$

Without a catalyst, the reaction proceeds very slowly and essentially stops with the addition of a few percent sodium

* Corresponding author. Tel.: +1 765 494 0061; fax: +1 765 494 0530.
E-mail address: zhengy@ecn.purdue.edu (Y. Zheng).

0378-7753/$ – see front matter © 2007 Elsevier B.V. All rights reserved.
doi:10.1016/j.jpowsour.2006.12.055

Nomenclature

d	diameter of the liquid droplet (m)
g	gravity constant (9.81 $m^2\ s^{-1}$)
V_f	velocity of the liquid droplet ($m\ s^{-1}$)

Greek letters

μ	viscosity of the fluid stream ($kg\ m^{-1}\ s^{-1}$)
ρ_f	density of the fluid stream ($kg\ m^{-3}$)
ρ_p	density of the liquid droplet ($kg\ m^{-3}$)

hydroxide to the solution (for long-term storage of sodium borohydride, a pH near 14 is desired). Therefore, sodium borohydride can be dissolved in water and transported stably as an aqueous solution. The solution can be used to generate hydrogen when pumped through a catalyst bed. The reaction products could then be transported to central facilities for regeneration.

Millennium Cell has conducted much research on this topic and published several papers [4–10]. Kojima et al. also have worked on this topic [11–16], and Jeong et al. have been working on the optimization of the catalyst for sodium borohydride hydrolysis [17]. Furthermore, a few studies have considered regeneration schemes [18–21]. In general, sodium borohydride systems are promising candidates for on-board hydrogen storage. Nevertheless, few groups have reported parametric system-level studies and some observations reported in the literature, such as hydrogen flow rate measurements for streams with high humidity and system performance at high fuel concentrations (higher than 20%), have not been independently verified.

Motivated by this, the objectives of this research were to construct a well-instrumented 1 kW_e subscale sodium borohydride system, to obtain experimental data especially temperature profiles inside the reactor under different controlled conditions, and to evaluate the feasibility of such a system for vehicle applications.

2. Experimental setup

2.1. Materials

To make $NaBH_4$ solutions, the desired amounts of $NaBH_4$ (Rohm Haas) and NaOH (Sigma–Aldrich) were weighed and loaded into the fuel tank. The desired amount of de-ionized water (laboratory grade) was then added together with vigorous stirring to enhance the dissolving process. Because dissolution of NaOH in water is exothermic, the solution temperature increased by as much as 8 °C. To prevent the fuel temperature from drifting during experiments due to cooling, the $NaBH_4$ solution was prepared several hours in advance to dissipate all the solution heat so that the fuel temperature was very near room temperature, approximately 22 °C. The $NaBH_4$ concentrations tested were 5%, 10%, 15% and 20%, and the NaOH concentration was 3%; the solution's pH was 14.

2.2. Setup

Fig. 1 shows a schematic of the sodium borohydride hydrogen generation system. Its scale is estimated to be of the order of one kilowatt (electrical) by assuming a 50% effi-

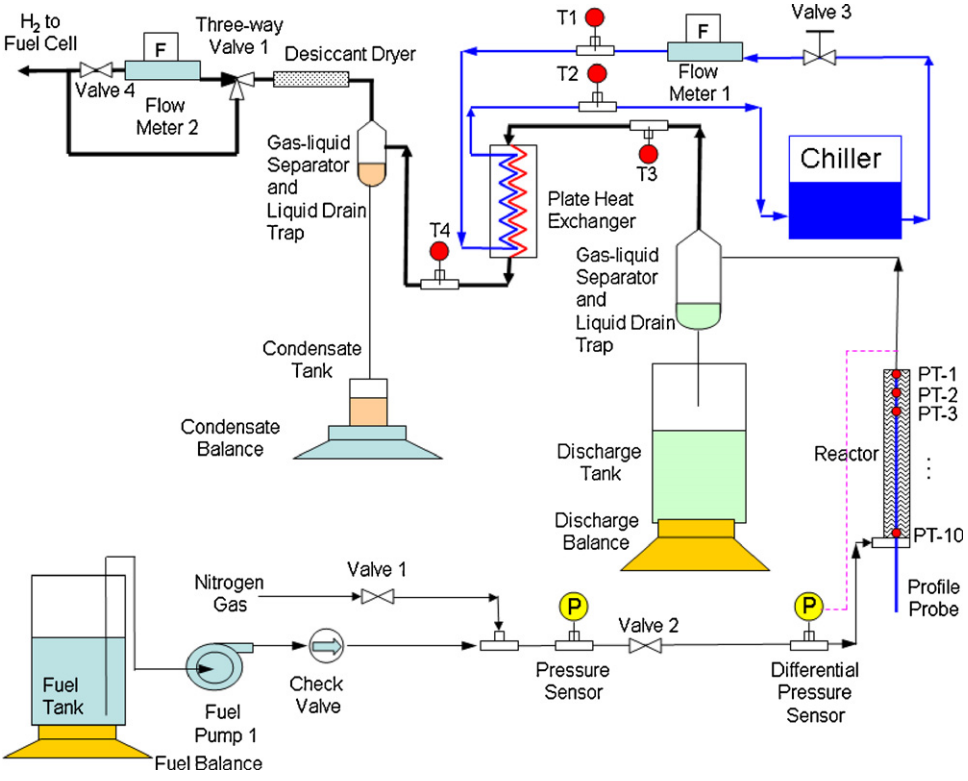

Fig. 1. Schematic of the 1 kW_e $NaBH_4$ hydrogen generation system.

ciency fuel cell. Sodium borohydride solution (fuel) is pumped through the packed-bed reactor, where the hydrolysis reaction initiates. The product stream consisting of gaseous hydrogen and liquid $NaBO_2$ solution is separated in a gas–liquid separator. The high-temperature hydrogen stream, containing a large amount of water vapor, undergoes a heat exchange process to condense the water vapor. Condensate in the hydrogen stream is separated and drained through another gas–liquid separator and liquid drain trap. Water vapor is further removed from the hydrogen stream through a desiccant dryer before the hydrogen stream passes through the flowmeter. The following sections discuss each major portion of the system in detail.

2.2.1. Tanks and corresponding balances

Fuel was pumped from a 1 gal stainless steel tank through a check valve to the reactor. Discharge product was collected in a tank, usually a glass container to enable visual observation. Similarly, condensate was collected in a glass container. To enable an accurate measurement of the fuel flow rate, a fuel balance was used to monitor the weight of the fuel during the experiment. The discharge and condensate tanks were monitored using balances as well.

2.2.2. Fuel pump

A gear pump installed on a digitally controlled programmable pump drive was used to flow sodium borohydride solution through the reactor. Gear pumps can deliver high pressure even when the flow rate is small. This feature is a significant advantage compared to centrifugal pumps, which typically can only deliver high pressures for high flow rates. The maximum flow rate of the pump is 250 mL min^{-1}, and the maximum differential pressure for continuous operation is 40 psi (2.75 bar), while the maximum differential pressure for intermittent operation is 60 psi (4.1 bar).

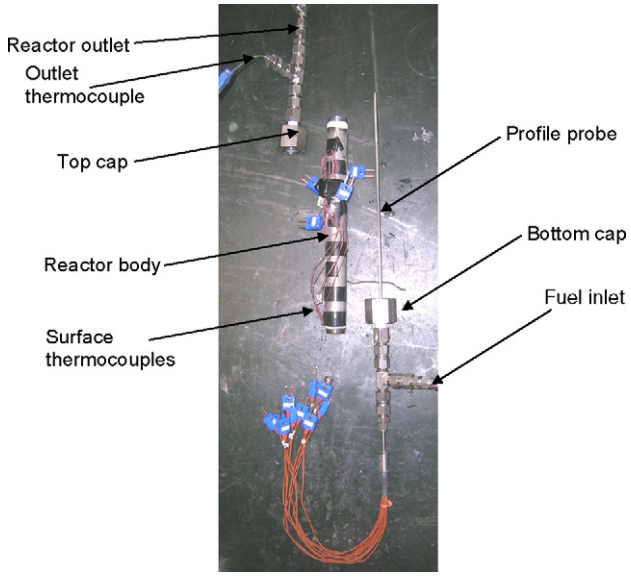

Fig. 2. Disassembled view of the reactor.

Table 1
Locations of thermocouples inside and outside the reactor

Name	Distance from the inlet (cm)
PT-1	28.7
PT-2	25.53
PT-3	22.35
PT-4	19.18
PT-5	16
PT-6	12.83
PT-7	9.65
PT-8	6.48
PT-9	3.3
PT-10	0.13
ST-1	25.53
ST-2	19.18
ST-3	16
ST-4	9.65
ST-5	3.3

2.2.3. Reactor

Fig. 2 shows the exposed view of the reactor. The inner diameter of the reactor is 2.09 cm. The height of the reactor is 28.7 cm, and the wall thickness is 2.9 mm. The reactor has an internal volume of 98 mL. The catalyst used was 3% 2 mm Ru on carbon extrudate (Johnson Matthey). The total mass of catalyst was 55.9 g, and the catalyst bed density was therefore 570 kg m^{-3}. At the inlet, a stainless steel fritz was used to retain the catalyst and to distribute inlet flow. A 1/8 in. (3.2 mm) hole was drilled through the fritz to insert a temperature profile probe into the reactor. The profile probe has ten type-T thermocouples (±0.5 °C) distributed evenly. The locations of all internal thermocouples designated as PT-* from the inlet are listed in Table 1. Five type-T thermocouples (±1.0 °C) were attached to the outside of the reactor to measure surface temperatures, and locations of all external thermocouples on the surface (designated as ST-*) are listed in Table 1 as well. The catalyst was packed from the top of the reactor, and the top was then capped using another stainless steel fritz. A NPT fitting was then installed to seal the system. To simplify future modeling, the reactor was well insulated with pipe insulation to simulate adiabatic operation conditions. All the downstream tubing and devices were also insulated.

2.2.4. Gas–liquid separator and liquid drain trap

Gas–liquid separators are widely used in the chemical industry; nevertheless, we could not find a device small enough for our bench reactor. As a result, we designed a custom gas–liquid separator with a design flow rate of 20 SLPM and an outlet droplet size smaller than 50 μm. By balancing the buoyant force of the droplet with the drag force, the following equation [22] for Stokes flow can be used to calculate the maximum diameter of droplets carried in the flow,

$$d = \sqrt{\frac{18\mu V_f}{(\rho_p - \rho_f)g}} \quad (2)$$

The gas–liquid separator body was designed with an inner diameter of 4 in. (10.2 cm) and height of 10 in. (25.4 cm). Two large 4 in. (10.2 cm) NPT caps were screwed on the 4 in.

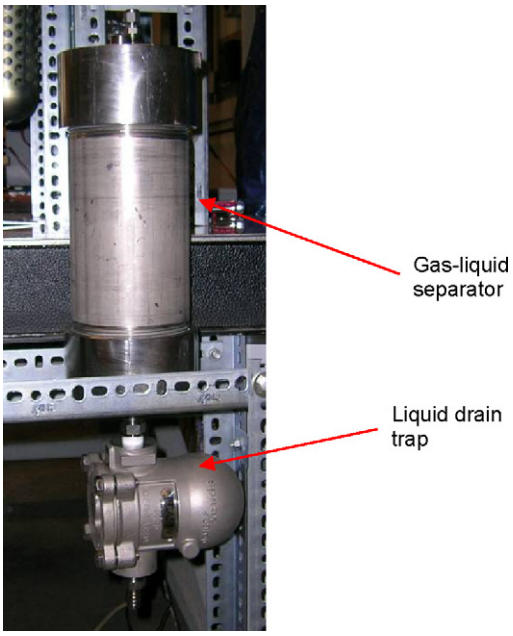

Fig. 3. Gas–liquid separator and liquid drain trap.

(10.2 cm) tube. Two 1/4 in. (0.635 cm) Swagelok fittings were welded to the top cap to serve as inlet and outlet ports. One 1/2 in. (1.27 cm) NPT fitting was welded on the bottom cap to serve as a liquid drain port to connect with the liquid drain trap installed below. As for the liquid drain trap, two Spirax Sarco CAS14 stainless steel liquid drain traps were used in the system. Fig. 3 contains a picture of the gas–liquid separator with the liquid drain trap.

2.2.5. Heat exchanger, chiller and cooling loop

A compact brazed-plate heat exchanger (SWEP, Inc.) was used to condense water vapor. Originally, a pre-filter and coalescing filter were installed upstream of the heat exchanger to capture small liquid droplets (containing sodium hydroxide that is corrosive to the heat exchanger) in the hydrogen stream escaping from the gas–liquid separator. Nevertheless, condensation inside the filters was found to be severe and required frequent manual draining, which could be unwanted during experiments. As a result, these items were removed from the system. Instead, a water line was installed so that heat exchanger could be flushed with water after each experiment to preserve its integrity.

To measure the amount of heat exchanged accurately, two high-precision thermistors (±0.01 °C) instead of thermocouples (±1.0 °C) were used to measure the inlet and outlet temperatures of chilled water inside the heat exchanger because a small temperature difference was expected. An air-cooled recirculating chiller was used as a cooling source for the heat exchanger. During experiments, the outlet water temperature was set to 5 °C, and the chilled water flow rate was set to 2.2 L min^{-1}.

2.2.6. Hydrogen conditioning station

Hydrogen must be conditioned before entering the flowmeter. Without conditioning, high-temperature hydrogen mixing with water vapor can easily condense inside the flowmeter and destroy the sensor. The flowmeter we used is based on the principle that pressure drop across a laminar flow element depends on flow rate and the viscosity of the gas. A small amount of water vapor in the hydrogen stream can significantly alter the viscosity of the mixture and affect the reading from the meter. Therefore, accurate measurement of the hydrogen flow must account for the presence of water vapor in the hydrogen stream. A silica gel-based desiccant dryer was used to remove water vapor in the hydrogen stream. A pre-filter and a coalescing filter were installed upstream the desiccant dryer for protection. An after-filter was installed downstream of the dryer to remove desiccant particulates carried in the gas stream.

2.2.7. Measurement of relative humidity of the hydrogen stream exiting the reactor

Because sodium borohydride hydrolysis is highly exothermic, water is vaporized and the amount of water vaporized has a strong effect on the temperature distribution inside the reactor as well as chemical kinetics. For reactor modeling purposes, it is very important to measure relative humidity for at least a few conditions to benchmark the reactor model. Sensors that directly measure the relative humidity of the hydrogen stream at high temperatures (80–120 °C) are not available. As a result, an indirect method was adopted. The condensate flow rate was used to estimate the relative humidity by assuming that the hydrogen stream coming out of the heat exchanger is saturated at the exit temperature. To make a meaningful estimate of relative humidity, the entire system must operate at the same condition for at least 30 min to reach thermal equilibrium. Applying an energy balance for the heat exchanger is not a trivial task because it requires waiting for a long time for the system to achieve thermal equilibrium; therefore, it was only conducted for a few conditions to extract relative humidity information for reactor modeling purposes.

2.2.8. Data acquisition system

A Keithley 2701 ethernet-based data acquisition system was used with two Keithley 7706 multiplexer cards to interface with 23 thermocouples and 10 analog inputs. The fuel pump was controlled by an analog output channel on the 7706 multiplexer card. A data acquisition program was developed using Labview 7 Express. The program graphically shows all the readings over time in addition to an instantaneous display of the temperature profile inside the reactor. These features are important because they reveal whether system has reached steady state and provide an estimate of conversion from the temperature profile, as explained in later sections. The balances were connected to the computer through a USB hub.

2.3. Chemical analysis

To measure the conversion of $NaBH_4$ directly and to verify the accuracy of the hydrogen flow rate reading, discharge solution was collected during experiments for chemical analysis. To enable accurate sampling of the discharge stream for analysis, it is imperative to collect the sample before the discharge stream goes to the gas–liquid separator, where it is mixed with

existing solution. An approximately 10 mL discharge sample was collected. The amount of unconverted $NaBH_4$ can be measured by the hydrogen collected inside a gas burette when the solution reacts with concentrated HCl. Approximately 3 mL of discharge sample and 1 mL of HCl were used. The exact amounts used were measured using an analytical balance before and after injection. Gas generated from the 1 kW_e system was verified to be hydrogen using gas chromatography.

2.4. System flushing

Because hydrogen is generated in the system, it is imperative that hydrogen does not mix with air inside the system. For safety reasons, the entire system must be purged with nitrogen before each experiment. Furthermore, because of potential crystallization of reaction products inside the system, reactor and liquid drain traps for the discharge stream must be flushed with water. In addition, because of the transport of sodium hydroxide into the heat exchanger, the heat exchanger also needs to be flushed with water.

3. Experimental results

3.1. Effects of flowrate

3.1.1. 10% $NaBH_4$

As shown in Fig. 4, at the low flow rate of 10 mL min^{-1}, a temperature plateau occurs near the reactor entrance, indicating that all the fuel is converted on the upstream side of the reactor. Also, even at the inlet, the temperature is already much higher than the initial fuel temperature of approximately 22 °C. With increasing fuel flow rate, the temperature at the inlet decreases significantly to approximately 22 °C, and the temperature rise inside the reactor is also less steep because of convective cooling from the fuel itself.

The location of the maximum temperature (hot spot) moves toward the outlet of the reactor with increased fuel flow rate. In addition, the maximum temperature inside the reactor also increases when the fuel flow rate increases up to 45 mL min^{-1}. This may be due to the fact that at lower flow rates, more water

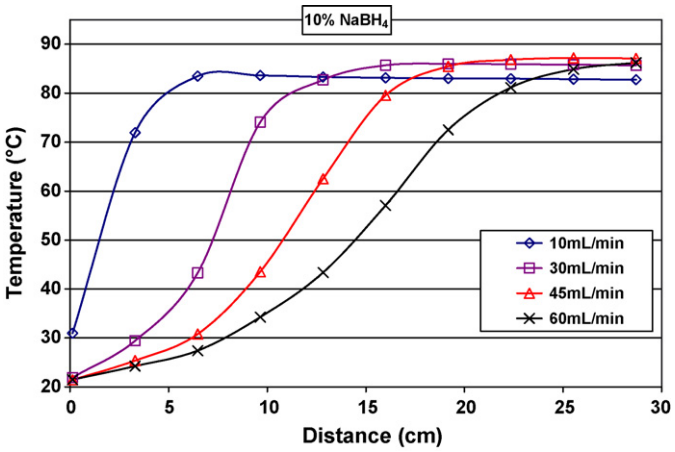

Fig. 4. Temperature distributions for 10% concentration at different flow rates.

Table 2
Measured data for 10% concentration at different flow rates

Set flow rate (mL min^{-1})	10	30	45	60
Flow rate (g min^{-1})	11.5	32.5	48.5	64.0
H_2 flow (SLPM)	2.9	8.8	12.8	14.8
Expected power (kW_e)[a]	0.24	0.72	1.05	1.21
System pressure (psig)	1.5	3.4	5.0	5.8
Differential pressure (psi)	0.8	2.0	3.0	3.2
Measured conversion (%)	100.0	100.0	97.4	83.5

[a] Calculated by assuming fuel cell efficiency of 50%.

is vaporized inside the reactor because of longer contact time. Therefore, more reaction heat is carried away via latent heat, and less reaction heat in the form of sensible heat results in lower exit temperature. Another possibility may be due to the imperfect insulation. More heat may be lost through the insulation for lower flow rates due to the fact that an elevated temperature exist through a larger portion of the reactor.

When the fuel flow rate increases to 60 mL min^{-1}, the temperature profile does not reach a plateau. Steep temperature gradients indicate high reaction rates, while a temperature plateau indicates a slow reaction rate or no reaction, implying complete conversion of reactant. Measured conversion data in Table 2 also confirm the foregoing reasoning. When the fuel flow rate is lower than 30mL min^{-1}, the temperature plateau is long, and the conversion is 100%. When fuel flow rate increases to 45 mL min^{-1}, the plateau is shorter, but the conversion is still high (97.4%). When the flow rate increases to 60 mL min^{-1}, no plateau occurs in the temperature profile and corresponding conversion is only 83.5%. Because of the difficulty of measuring chemical conversion, the above observations can be used to indicate chemical conversion qualitatively via the temperature profile. A large temperature gradient at the outlet implies low conversion, while a small temperature gradient at the outlet implies high conversion.

3.1.2. 5% $NaBH_4$

Temperature distributions for the 5% concentration tests follow a similar trend to those observed for the 10% tests. Nevertheless, because of the decreased concentration and decreased amount of heat generated, the maximum temperature inside the reactor reached approximately 75 °C compared to approximately 85 °C for 10% concentration. For the same 10 mL min^{-1} flow rate, the initial temperature increase is much less steep than that for 10% concentration. Furthermore, a much lower flow rate is needed to push the temperature plateau out of the reactor (30 mL min^{-1} for 5% compared to approximately 60 mL min^{-1} for 10%).

3.1.3. 15% $NaBH_4$

With 15% fuel, the higher concentration results in a larger rate of heat generation as indicated in Fig. 5 and Table 3. At the 10 mL min^{-1} flow rate, the temperature at the inlet reaches approximately 55 °C, which is much higher than the 30 °C observed for 10% fuel at 10 mL min^{-1} flow rate. For the 30 mL min^{-1} flow rate, the initial temperature increase is still rather large. Flow rates higher than 30 mL min^{-1} result in a

Table 3
Measured data for 15% concentration at different flow rates

Set flow rate (mL min^{-1})	10	20	30	40	50	60	80
Flow rate (g min^{-1})	11.4	21.7	32.3	43.0	53.2	64.3	81.3
H_2 flow (SLPM)	4.8	8.9	12.7	16.9	20.13	22.66	22.93
Expected power (kW_e)[a]	0.39	0.73	1.04	1.38	1.65	1.85	1.88
System pressure (psig)	2.8	5.4	8.1	11.1	13.1	14.4	13.8
Differential pressure (psi)	1.6	3.2	4.4	5.8	6.7	6.8	6.0
Measured conversion (%)	100.0	100.0	99.0	99.0	95.0	88.0	70.0

[a] Calculated by assuming fuel cell efficiency of 50%.

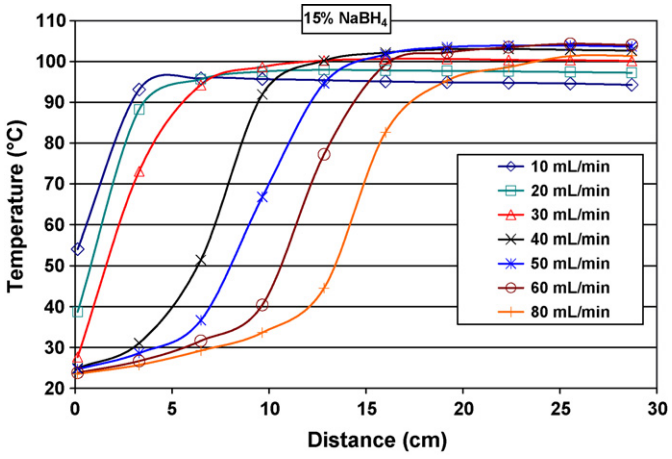

Fig. 5. Temperature distributions for 15% concentration at different flow rates.

significant change in the temperature profile in that the initial temperature increase moderates. The overall trend was the same with 10% fuel. That is, higher flow rates result in a slow temperature rise in the entry section and a more rapid increase of temperature downstream.

3.1.4. 20% $NaBH_4$

In the initial two tests using 20% concentration solution, we attempted to warm the catalyst bed by pumping 20% solution at a 10 mL min^{-1} flow rate. Surprisingly, the system did not reach a steady-state condition. At the end of the experiment, the system pressure kept increasing, together with reactor temperature. The experiment was stopped when the system pressure reached almost 60 psig—the maximum pressure provided by the pump. Disassembly of the system revealed that the discharge sampling station was almost completely blocked by solid crystals that caused the system pressure to increase. Later, we successfully operated the reactor using 20% concentration by warming up the system using 15% concentration and by pressurizing the system to achieve a higher operating temperature. The temperature profiles for 20% concentration at different flow rates follow the trend observed for 15% concentration and are not shown here for brevity.

3.2. Effects of inlet heating

For 10% $NaBH_4$ solution, Fig. 6 shows clearly that with inlet heating under a flow rate of 60 mL min^{-1}, the reaction rate at the entry section increases significantly. Therefore, the temperature profile reaches a plateau much earlier. The measured conversion increased significantly from 83.5% to 95.4% due to inlet heating. The significance of this result is that conversion of $NaBH_4$ inside the reactor can be improved by heating the inlet stream with the discharge stream through a heat exchanger or by using the waste heat from the fuel cell. Without inlet heating, the length of the reactor must be increased to achieve the same conversion, but such a change would increase the cost of the reactor because more catalyst and reactor volume would be required.

3.3. Effects of pressure

Fig. 7 shows that for 10% concentration and increased system pressures under a 60 mL min^{-1} flow rate, the maximum temperature inside the reactor increases as expected because the saturation temperature (boiling point) of the aqueous solution increases with system pressure. Interestingly, the temperature in most of the reactor is lower for higher system pressures. Furthermore, the temperature gradient at the outlet of the reactor increases with operating pressure, implying that more $NaBH_4$ is unreacted in the discharge stream. Measured conversion data listed in Table 4 confirm the trend observed in the temperature profile, i.e., that conversion decreases with increased system pressure.

This phenomenon is contrary to intuition. Generally, reactor temperature would be expected to increase with pressure. As a result, the kinetics should be faster, and the overall conversion should be higher. For the $NaBH_4$ reaction, however, the situation is more complicated. Because the reaction involves the gen-

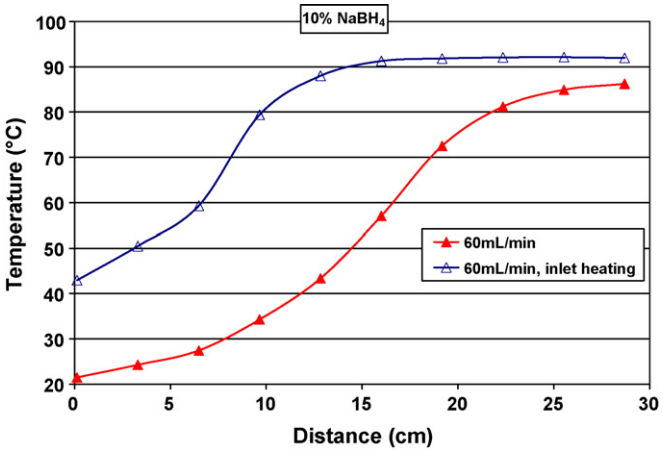

Fig. 6. Temperature distributions for 10% concentration with inlet heating condition.

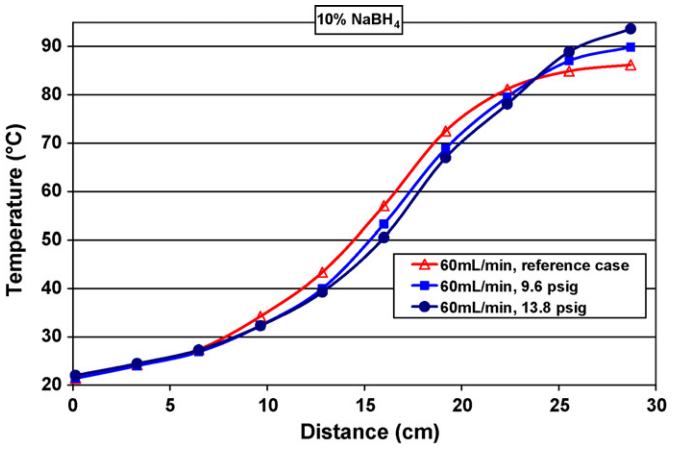

Fig. 7. Temperature distributions for 10% concentration under different pressure conditions.

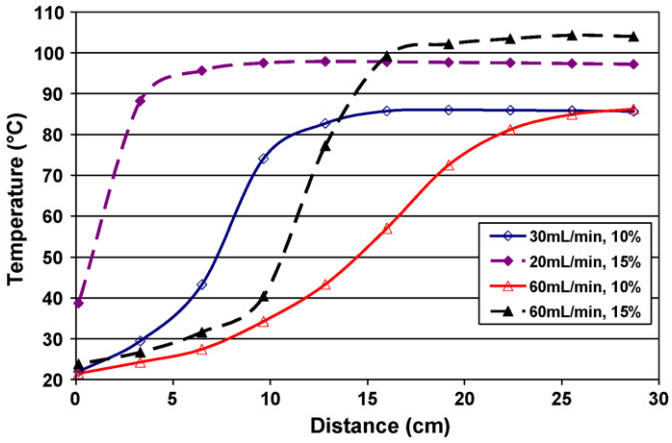

Fig. 8. Temperature distributions for different concentrations.

eration of hydrogen, increased pressure may push equilibrium toward the reactants and result in lower conversion. Another possibility is that higher operating pressure may increase the channelling of fuel solution through the reactor without reaction, and as a result, total conversion would be lower. Guo and Al-Dahhan [23] also reported lower conversion at higher pressures in a gas–liquid co-current downflow packed-bed reactor and showed that the decrease in conversion originated from lower liquid flow resistance inside the reactor at elevated pressure. Tests with 15% $NaBH_4$ under pressure conditions also confirmed the trend with 10% solution—that is, decreased conversion with increased pressure.

3.4. Effects of concentration

Fig. 8 shows two comparisons. The first comparison is between 30 mL min^{-1} of 10% solution and 20 mL min^{-1} of 15% solution for which the total hydrogen generation rates are the same. Because of higher concentration and lower cooling effects for the lower flow rate (20 mL min^{-1}), the upstream temperature increases rapidly, and the temperature profile reaches a plateau much earlier than that for the 30 mL min^{-1} case. This result shows the benefit associated with higher concentrations. Another comparison is between 60 mL min^{-1} of 10% solution and 60 mL min^{-1} of 15% solution. We note that initially, the temperature profiles are quite similar because of the high convective cooling effect at high flow rates. Then, 10 cm downstream from the inlet, the temperature for the higher concentration begins to increase rapidly, while the temperature for the lower concentration increases much more slowly because increased concentration results in higher reaction rates and therefore more rapid temperature increases. The result shows the benefit associated with higher concentrations even at higher flow rates.

Table 4
Measured data for 10% concentration under different system pressures

System pressure (psig)	5.8 (reference case)	9.6	13.8
Set flow rate (mL min^{-1})	60	60	60
Flow rate (g min^{-1})	64.0	64.0	64.0
H_2 flow (SLPM)	14.8	14.1	13.7
Expected power (kW_e)[a]	1.21	1.15	1.12
Differential pressure (psi)	3.2	2.4	1.8
Measured conversion (%)	83.5	80.2	78.2

[a] Calculated by assuming fuel cell efficiency of 50%.

3.5. Relative humidity of the hydrogen stream

We measured relative humidity by condensing the hydrogen stream with a heat exchanger, measuring the amount of condensate and then deducing the relative humidity. Relative humidity measurements were only conducted for a few conditions using 10% solution and are listed in Table 5. Because this method of measurement is complicated, we estimate the uncertainty to be approximately ±10%, compared to ±5% for most relative humidity transducers. We note from Table 5 that relative humidity at the exit of the reactor is not 100%, which confirms the need to conduct relative humidity measurements. The exiting relative humidity decreases with increasing flow rate, perhaps due to the decreasing length of the temperature plateau in the reactor. The exiting relative humidity increases under inlet heating condition, which is reasonable because more heat was added to the system and a longer temperature plateau was observed.

3.6. Degradation of the catalyst bed

Fig. 9 shows that the temperature profile shifts downstream over time, indicating a temporal degradation of catalyst activity. Table 6 shows the measured hydrogen flow rates and measured conversions at different times for a fuel flow rate of 45 mL min^{-1} with 10% $NaBH_4$. These results suggest that the catalyst used in this project was not optimal for $NaBH_4$ hydrolysis. Other researchers have also reported degradation tests [13,24], but it is unclear whether the flow rate used was large enough to reach a firm conclusion. For low flow rates, measurements of total

Table 5
Measured relative humidity for 10% concentration

Set flow rate (mL min^{-1})	45	60	60
Inlet temperature (°)	20.3	20.5	42.5 (inlet heating)
RH of H_2 stream (%)	69.9	62.7	87.9

Table 6
Degradation of conversion with time

Time (min)	20	50	80	110	140	170	210	240	280
Set flow rate ($g\,min^{-1}$)	49.5	49	48.5	46.5	47	51	49	49.00	49.50
H_2 flow (SLPM)	12.12	11.60	11.29	10.72	10.90	10.84	10.39	10.29	10.20
Expected power (kW_e)[a]	0.99	0.95	0.92	0.88	0.89	0.89	0.85	0.84	0.83
Measured conversion (%)	87.7	85.1	82.3	79.0	77.6	70.8	73.5	72.6	71.6

[a] Calculated by assuming fuel cell efficiency of 50%.

hydrogen generated may not reveal degradation even when it exists because to measure degradation, the flow rate must be large enough so that the conversion is less than 100%.

3.7. Surface temperature and validity of the one-dimensional assumption

Surface temperatures of the reactor were recorded and compared to the temperature profile inside the reactor. It was found that surface temperatures track interior temperatures very closely, within 2 °C for most cases. These results therefore indicate that it is reasonable to assume a one-dimensional temperature distribution inside the reactor for modeling purposes.

3.8. Crystallization of discharge product

Section 3.1.4 first discussed issues with product crystallization. Fig. 10 shows a side-by-side comparison of discharged product collected for two concentrations experiments. The left image is for 20% solution, and the right one is for 15% solution. As shown, all the product crystallized. Once the discharge solution crystallized, it adhered to the wall of the container and became very difficult to remove. Considering the challenges in maintaining a practical discharge tank at high temperatures to prevent discharge crystallization, especially when a vehicle is parked for a long time, we believed that 10–15% $NaBH_4$ is the maximum concentration that can be used reliably, corresponding to a maximum of 3.1 wt.% for the solution material itself.

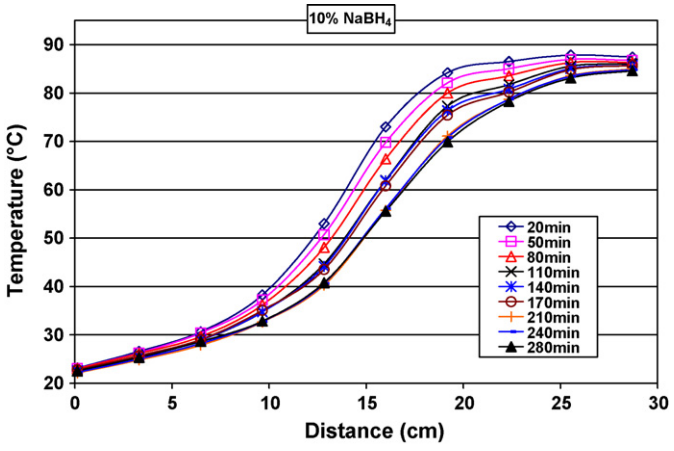

Fig. 9. Degradation of total conversion implied by a shift in temperature over time with 10% $NaBH_4$ at 45 mL min^{-1}.

Fig. 10. Discharge products (left for 20% solution and right for 15% solution).

4. Discussion

4.1. Measurement of hydrogen flow rate

The flowmeter used in the present experiments employs the principle of pressure drop across a laminar element that is sensitive to the flow rate and the viscosity of the gas, and its calibration is based on pure hydrogen. When used in a chemical hydride system, the hydrogen stream must be dried first to remove water; otherwise, water vapor inside the hydrogen stream will significantly increase the viscosity of the gas and strongly affect the pressure drop. Furthermore, because the hydrogen stream is at high temperature, when it passes through the flowmeter without condensing, water can condense inside the flowmeter and destroy the sensing element. The study by Kojima et al. [13] did not mention condensing the hydrogen stream before measuring its flow rate; as a result, their reported flow rate may be significantly higher than actual values.

4.2. $NaBO_2$ solubility phase diagram

During experiments, we noticed that different types of $NaBO_2$ formed under different test conditions. The discharge solution using 10% fuel crystallized after exposure to air for several weeks. The crystal was clear and transparent. Through X-ray and elemental analysis, we found that the crystal was $NaBO_2{\cdot}4H_2O$. The discharge solution using 20% fuel crystallized shortly after cooling, and the crystal was white and opaque. Through X-ray and elemental analysis, we found that the crystal was similar to $NaBO_2{\cdot}2H_2O$.

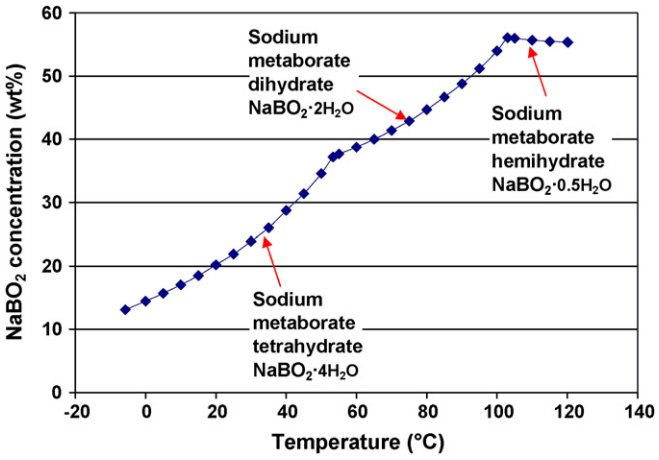

Fig. 11. Solubility phase diagram of $NaBO_2$ in water, adapted from Ref. [25].

We have plotted solubility data of $NaBO_2$ covering the range of −5.77 to 120.2 °C in Fig. 11 [25], which shows that three different crystals may be formed from sodium borate solution depending on the solution temperature at which the crystal is formed. Below 53.3 °C, tetrahydrate ($NaBO_2{\cdot}4H_2O$) is formed. Between 53.3 and 103.0 °C, dihydrate ($NaBO_2{\cdot}2H_2O$) is formed. Above 103.0 °C, hemihydrate ($NaBO_2{\cdot}0.5H_2O$) is formed. Blasdale and Slansky [26] indicated that obtaining pure dihydrate was very difficult, and typical products were a mixture of dihydrate and tetrahydrate. The solubility curve shows that the maximum $NaBO_2$ concentration is 56.1 wt% at 103.0 °C. Above that temperature, solubility decreases slightly.

The boiling point of the $NaBO_2$ solution is 120.2 °C. Above that temperature, the solution begins to boil, and the crystals will melt. Therefore, solubility becomes very difficult to define. Nevertheless, according to Blasdale and Slansky [26], above 70 °C, saturated solutions become very viscous and assume a glass-like character similar to solutions of sodium silicate. When the reactor operates at temperature higher than 120.2 °C (achieved by pressurizing the reactor), $NaBO_2$ solution becomes a solution or slurry due to the melting of the crystal. As a result, the reactor in general will not have solubility issues. Nevertheless, once $NaBO_2$ solution exits the reactor and begins to cool, it may immediately crystallize and cause problems in the system as discussed in Section 3.1.4.

In principle, adding some chemicals may increase the solubility of $NaBO_2$. Unfortunately, the solubility of $NaBO_2$ decreases rather than increases in the presence of common additives, such as NaOH and NaCl, probably because of competition for water. An economical solution to this problem is highly desired for the application of sodium borohydride based on-board hydrogen storage systems.

From our experience, once crystallization begins, crystals adhere to the wall of the container very tightly, much like glue. As a result, removing the crystal from the container is very difficult. Should crystallization occur inside a vehicle discharge tank, the product would become very difficult to remove. Furthermore, with a high concentration of $NaBH_4$, the reactor must be flushed with abundant water after usage; otherwise, when the reactor cools, the residual $NaBO_2$ may cover the catalyst and destroy the reactor. Installing an extra water tank to purge the system after each operation will further increase the complexity of the system and decrease the overall weight and volumetric densities.

5. Conclusions

From the present test results, we believe that 15% $NaBH_4$ appears to be the maximum concentration that can be used in vehicle applications without adding extra and costly provisions for the discharge stream. For concentrations above 15%, special care is required for the discharge stream. For concentrations above 20%, the potential for thermal runaway exists. Fifteen percent solution results in a material weight percentage of 3.1 wt% hydrogen, and therefore, we conclude that $NaBH_4$ hydrolysis would not satisfy DOE Freedom Car target for 2010 of 6.0 wt%.

The systematic study of a $NaBH_4$ system reported here also suggests that similar solubility issues may exist for other chemical hydride systems such as NaH, MgH_2 and $LiBH_4$ when maximum hydrogen storage density is desired. In a feasible chemical hydride system for automotive applications, reactants should be able to be introduced into the reactor readily. In this respect, liquid-phase reactants are highly desirable because of difficulties in dispensing solid reactants into pressurized reactors. Because most hydrolysis reactions are exothermic, reaction heat must be removed from the system continuously to prevent thermal runaway. Furthermore, in a flow system, continuous removal of reaction products is also crucial and requires the reaction products to be either liquid or solids that are highly soluble in the solvent used in the reaction. Simultaneously satisfying all the three requirements to achieve a reliable engineering system will be extremely challenging.

Acknowledgement

The primary author thanks Prof. Nick Delgass in Purdue's School of Chemical Engineering for insightful discussions.

References

[1] U.S. Department of Energy, Office of Basic Energy Sciences, Basic research needs for the hydrogen economy, 2003 (report available at: http://www.sc.doe.gov/bes/hydrogen.pdf).
[2] U.S. Department of Energy, Office of Hydrogen, Fuel Cells, and Infrastructure Technologies, Multi-year research, development and demonstration plan, 2003 (report available at: http://www.eere.energy.gov/hydrogenandfuelcells/mypp/).
[3] J.S. Zhang, T.S. Fisher, P.V. Ramachandran, J.P. Gore, I. Mudawar, J. Heat Transfer 127 (2005) 1391–1399.
[4] S.C. Amendola, S.L. Sharp-Goldman, M.S. Janjua, M.T. Kelly, P.J. Petillo, M. Binder, J. Power Sources 85 (2000) 186–189.
[5] S.C. Amendola, S.L. Sharp-Goldman, M.S. Janjua, N.C. Spencer, M.T. Kelly, P.J. Petillo, M. Binder, Int. J. Hydrogen Energy 25 (2000) 969–975.
[6] R.M. Mohring, R.E. Luzader, SAE paper 2001-01-2529.
[7] R.M. Mohring, I.A. Eason, K.A. Fennimore, SAE paper 2002-01-0098.
[8] R.M. Mohring, Y. Wu, Proceedings of the First International Workshop on Hydrogen in Materials and Vacuum Systems, Newport News, Virginia, November 11–13, 2002, pp. 90–100.
[9] M. Kelly, A. Briggs, Proceedings of the International Telecommunications Energy Conference, Montreal, Canada, September 29–October 3, 2002, pp. 331–337.

[10] V. Hovland, A. Pesaran, R.M. Mohring, I.A. Eason, G.M. Smith, D. Tran, R. Schaller, T. Smith, SAE paper 2003-01-2271.
[11] Y. Kojima, K. Suzuki, K. Fukumoto, M. Sasaki, T. Yamamoto, Y. Kawai, H. Hayashi, Int. J. Hydrogen Energy 27 (2002) 1029–1034.
[12] Y. Kojima, Y. Kawai, H. Nakanishi, S. Matsumoto, J. Power Sources 135 (2004) 36–41.
[13] Y. Kojima, K. Suzuki, K. Fukumoto, Y. Kawai, M. Kimbara, H. Nakanishi, S. Matsumoto, J. Power Sources 125 (2004) 22–26.
[14] Y. Kojima, K.I. Suzuki, Y. Kawai, J. Mater. Sci. 39 (2004) 2227–2229.
[15] Y. Kojima, Y. Kawai, M. Kimbara, H. Nakanishi, S. Matsumoto, Int. J. Hydrogen Energy 29 (2004) 1213–1217.
[16] Y. Kojima, K.-i. Suzuki, Y. Kawai, J. Power Sources 155 (2006) 325–328.
[17] S.U. Jeong, R.K. Kim, E.A. Cho, H.-J. Kim, S.-W. Nam, I.-H. Oh, S.-A. Hong, S.H. Kim, J. Power Sources 144 (2005) 129–134.
[18] S. Suda, in: W. Vielstich, H.A. Gasteiger, A. Lamm (Eds.), Handbook of Fuel Cells—Fundamentals, Technology and Applications, John Wiley & Sons, Hoboken, NJ, 2003, pp. 115–120.
[19] Y. Kojima, T. Haga, Int. J. Hydrogen Energy 28 (2003) 989–993.
[20] D. Bingham, K. Wendt, B. Wilding, Proceedings of 2004 Annual U.S. DOE Hydrogen Program Review, 2004, http://www.eere.energy.gov/hydrogenandfuelcells/2004_annual_review.html.
[21] Y. Wu, Proceedings of 2004 Annual U.S. DOE Hydrogen Program Review, 2004, http://www.eere.energy.gov/hydrogenandfuelcells/2004_annual_review.html.
[22] J.A. Fay, Introduction to Fluid Mechanics, MIT Press, Cambridge, MA, 1994.
[23] J. Guo, M. Al-Dahhan, Chem. Eng. Sci. 59 (2004) 5387–5393.
[24] Q. Zhang, G. Smith, Y. Wu, R. Mohring, Int. J. Hydrogen Energy 31 (2006) 961–965.
[25] D.E. Garrett, Borates: Handbook of Deposits, Processing, Properties, and Use, Academic Press, San Diego, CA, 1998.
[26] W.C. Blasdale, C.M. Slansky, J. Am. Chem. Soc. 61 (1939) 917–920.